Electronic Supplemental Information for

Successive surface engineering of TiO_2 compact layer via dual modification of fullerene derivatives affording hysteresis-suppressed high-performance perovskite solar cells

Weiran Zhou, Jieming Zhen, Qing Liu, Zhimin Fang, Dan Li, Pengcheng Zhou,

Tao Chen*, and Shangfeng Yang*

Hefei National Laboratory for Physical Sciences at Microscale, Key Laboratory of Materials for Energy Conversion, Chinese Academy of Sciences, Department of Materials Science and Engineering, Synergetic Innovation Center of Quantum Information & Quantum Physics, University of Science and Technology of China (USTC), Hefei 230026, China

Contents

S1. UV-vis absorption and XPS spectra of $PC_{61}BM$ and C_{60}-ETA films before and after DMSO washing.

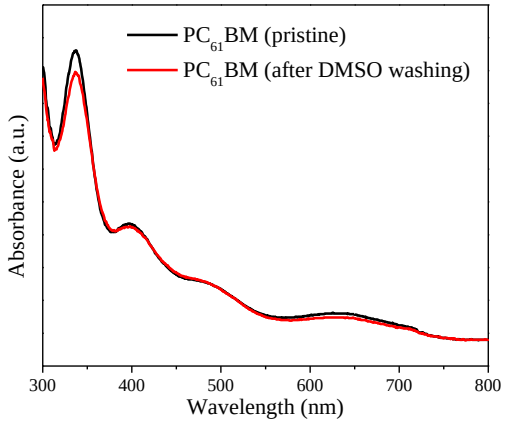

Figure S1. UV-vis absorption spectra of $PC_{61}BM$ film before and after DMSO washing.

After fabricating the $PC_{61}BM$ layer on FTO/TiO_2 substrate, pure DMSO solvent was spin-coated onto the $PC_{61}BM$ layer at 4000 rpm for 30 s (exactly identical to the condition used for spin-coating PbI_2/DMSO solution during device fabrication). According to the comparison of the UV-vis spectra of $PC_{61}BM$ film before and after DMSO washing, all characteristic absorption peaks are clearly observed despite of the small decreases of the intensities of several peaks (see Fig. S1). This indicates that $PC_{61}BM$ layer may be partially washed out by DMSO, while most materials in the $PC_{61}BM$ layer still remains on the substrate.

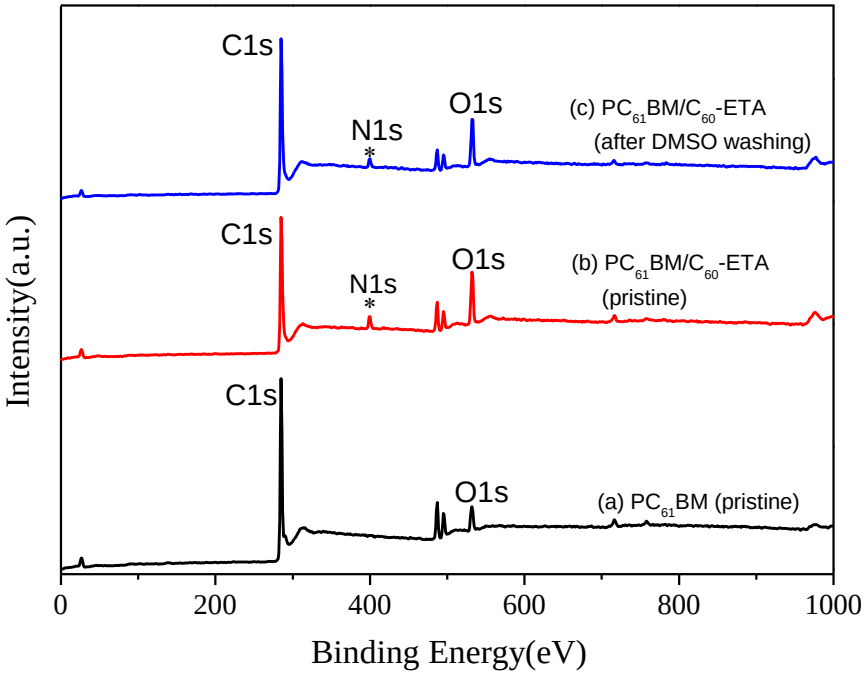

Figure S2. XPS spectra of $PC_{61}BM/C_{60}$-ETA film before and after DMSO washing in comparison with that of $PC_{61}BM$ film.

C_{60}-ETA layer was spin-coated onto the $PC_{61}BM$ layer on FTO/TiO_2 substrate, and DMSO solvent treatment was carried out by spin-coating pure DMSO solvent onto the $PC_{61}BM/C_{60}$-ETA film at 4000 rpm for 30 s. According to the comparison of the XPS survey spectra of $PC_{61}BM/C_{60}$-ETA film before and after DMSO washing (see Fig. S2), the N1s signal detected for the pristine $PC_{61}BM/C_{60}$-ETA film (curve b) is still detected in the XPS survey spectrum of the film after DMSO washing (curve c). Since C_{60}-ETA is the only source of N element (which is absent in the spectrum of $PC_{61}BM$ film, curve a), these results confirm that C_{60}-ETA layer remains on $PC_{61}BM$ layer after DMSO washing.

S2. Estimated void ratios of $CH_3NH_3PbI_3$ films fabricated on different substrates.

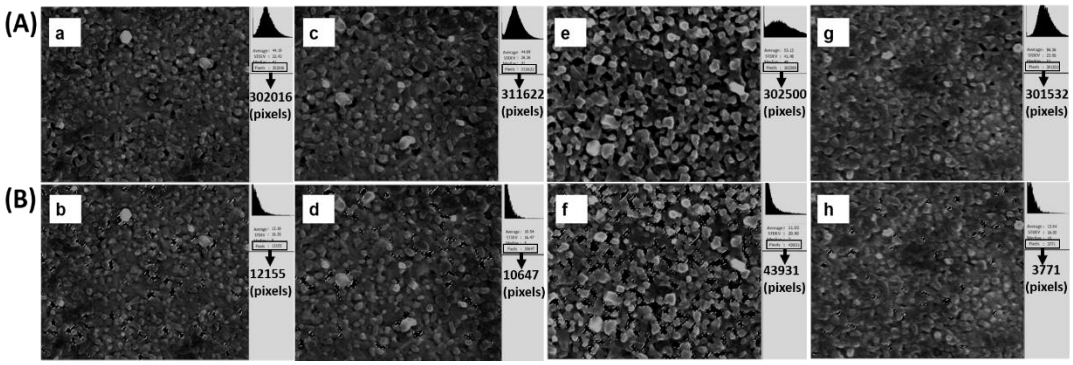

Figure S3. The pixels of whole area (A) and the pinhole area (B) of $CH_3NH_3PbI_3$ films fabricated on TiO_2 (a, b), TiO_2/C_{60}-ETA (c, d), TiO_2/$PC_{61}BM$ (e, f) and TiO_2/$PC_{61}BM$/C_{60}-ETA (g, h) ETLs.

Table S1. The estimated void ratios of $CH_3NH_3PbI_3$ films fabricated on different ETLs.

ETL	Total pixels of the pinhole areas	Total pixels of the whole area	Void (pinhole) ratio [a]
TiO_2	12155	302016	4.02%
TiO_2/C_{60}-ETA	10647	311622	3.42%
TiO_2/$PC_{61}BM$	43931	302500	14.52%
TiO_2/$PC_{61}BM$/C_{60}-ETA	3771	301532	1.25%

[a] Void (pinhole) ratio = Total pixels of the pinhole areas / Total pixels of the whole area.

S3. AFM images of different substrates.

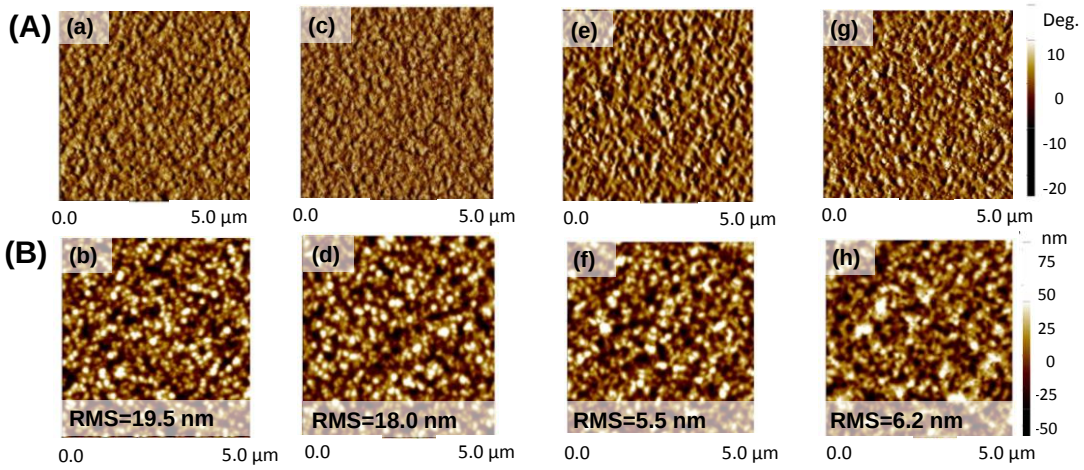

Figure S4. AFM phase (A) and the corresponding height (B) images of pristine TiO_2 (a, b), TiO_2/C_{60}-ETA (c, d), TiO_2/$PC_{61}BM$ (e, f) and TiO_2/$PC_{61}BM$/C_{60}-ETA (g, h) films.

S4. UV-vis absorption spectra of different substrates and the corresponding perovskite films.

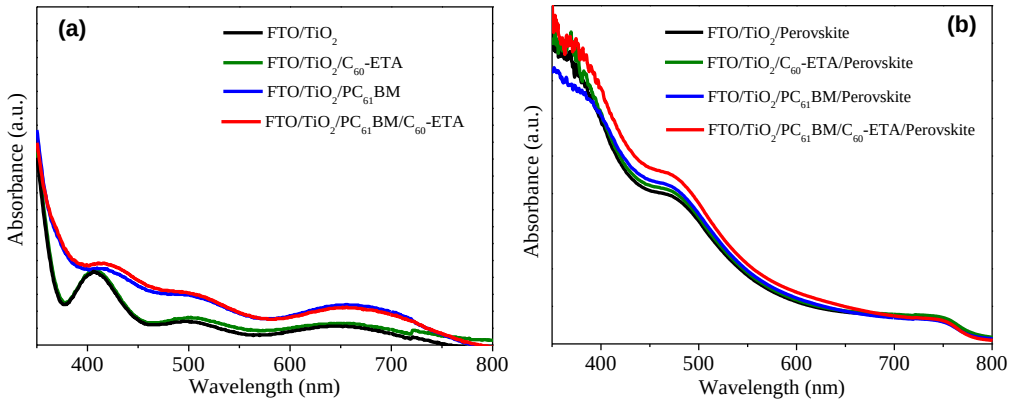

Figure S5. UV-vis absorption spectra of different substrates (a) and the corresponding perovskite films (b).

S5. Estimation of the energy levels of C_{60}-ETA.

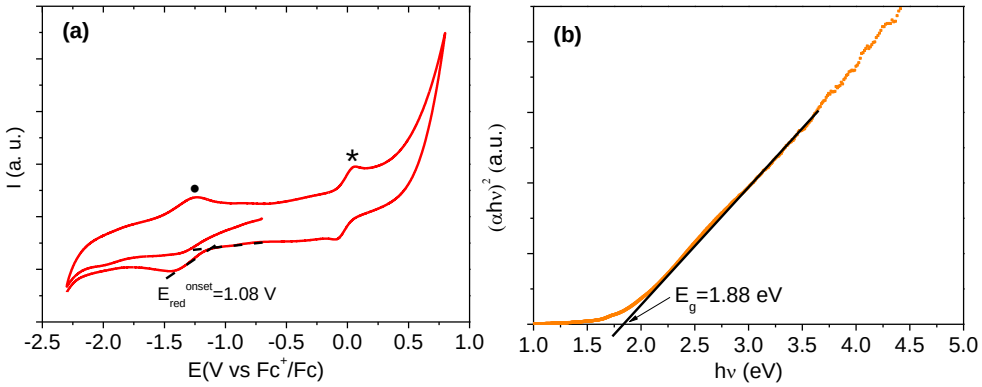

Figure S6. (a) Cyclic voltammogram of C_{60}-ETA in DMSO solution with ferrocene (Fc) as the internal standard. Scan rate: 100 mV/s, $TBAPF_6$ as supporting electrolyte. The asterisk labels the oxidation peak of ferrocene. (b) Tauc's law plot of the absorption coefficient of C_{60}-ETA deposited on a glass substrate.

The lowest unoccupied molecular orbital (LUMO) and highest occupied molecular orbital (HOMO) of C_{60}-ETA was determined by cyclic voltammetric study and diffuse reflectance spectroscopy. The cyclic voltammetric study was performed on a CHI 660D potentiostat (CHI Instrument, USA) in dimethyl sulfoxide (DMSO) with tetrabutylamonium hexafluorophosphate ($TBAPF_6$, Puriss. electrochemical grade, Fluka) as supporting electrolyte. A standard three-electrode arrangement of a platinum (Pt) wire as working electrode, a platinum coil as counter electrode, and a silver wire as a pseudo-reference electrode was used. In comparison, ferrocene (Fc) was added as the internal standard and all potentials are referred to Fc/Fc^+ couple which owes an absolute energy level of -4.8 eV to vacuum. As depicted in Figure S6a, the onset reduction potentials (E_{red}^{onset}) of C_{60}-ETA was estimated to be -1.08 V vs Fc^+/Fc (which has a half-wave oxidation potential ($E_{1/2}$) at 0.70 V vs Ag^+/Ag). Hence the LUMO energy level of C_{60}-ETA is -3.72 eV calculated by $E_{LUMO}=-e(E_{red}^{onset} + 4.8)$.[S1,S2]

As is seen in Fig. S6a, there is no oxidation peak was observed in the cyclic voltammogram of C_{60}-ETA, so the HOMO energy level of C_{60}-ETA is calculated by $E_{HOMO}=E_g^{opt} - E_{LUMO}$, and E_g^{opt} is the optical bandgap. The bandgap (E_g^{opt}) is estimated

by diffuse reflectance spectroscopy (Figure S6b), the conventional Tauc's law $(\alpha h\nu)^2$ as a function of the photon energy hν. The E_g of C_{60}-ETA is estimated to be 1.88 eV according to the extrapolation of the linear part of this curve.[S3] Thus HOMO energy level of C_{60}-ETA is eatimated to be -5.60 eV calculated by $E_{HOMO}=E_g - E_{LUMO}$.

S6. Determination of the thickness of the C_{60}-ETA.

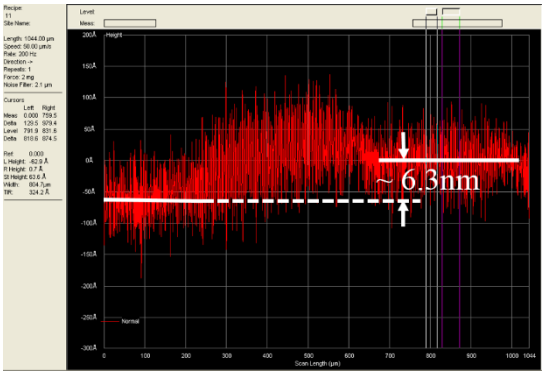

Figure S7. Surface profile of C_{60}-ETA measured on KLA-Tencor P6 surface profilometer. The thickness of C_{60}-ETA layer is ~6.3 nm.

S7. Box plots of photovoltaic parameters.

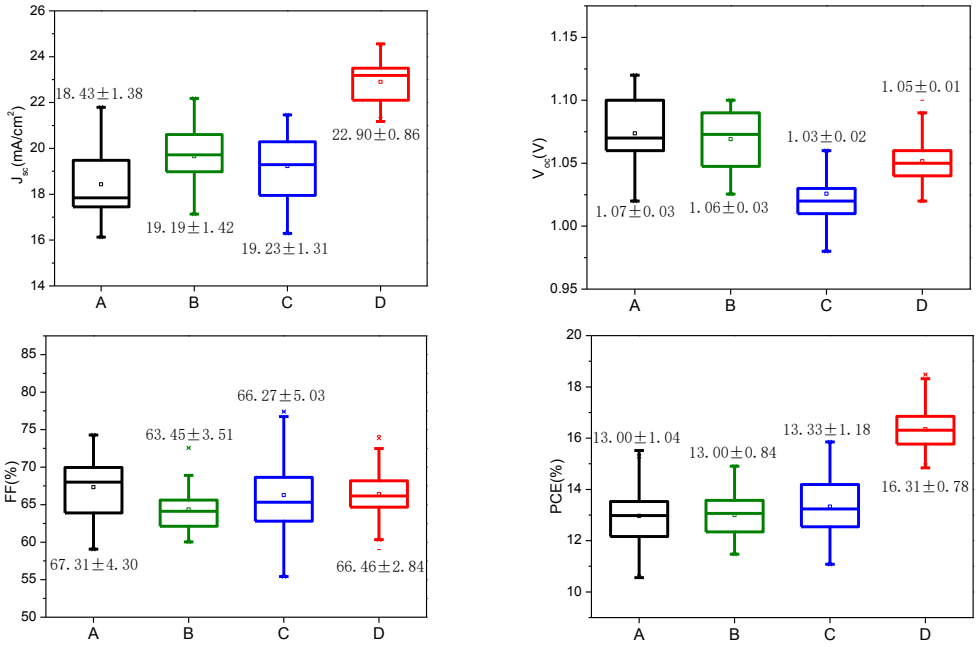

Figure S8. Photovoltaic parameters extracted from current-voltage measurements of devices **A**, **B, C,** and **D**.

S8. PCE histograms of devices A and D.

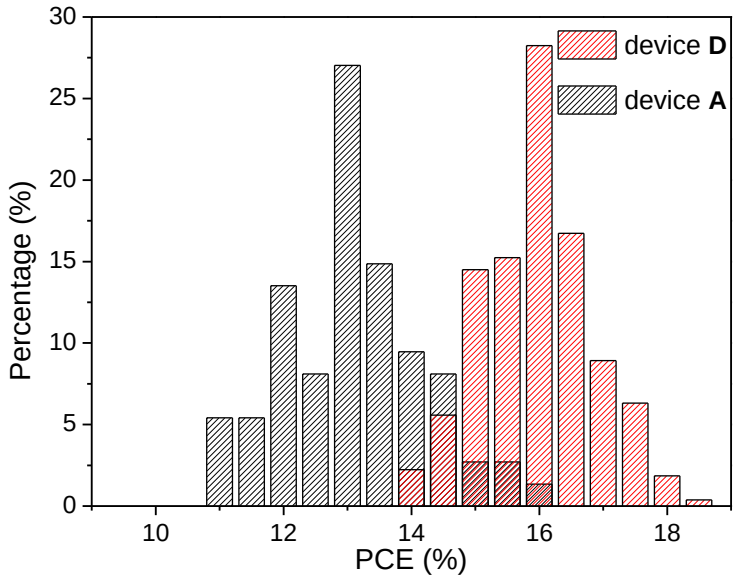

Figure S9. PCE histograms of devices **A** and **D**.

S9. Stabilized current density and power output of device D.

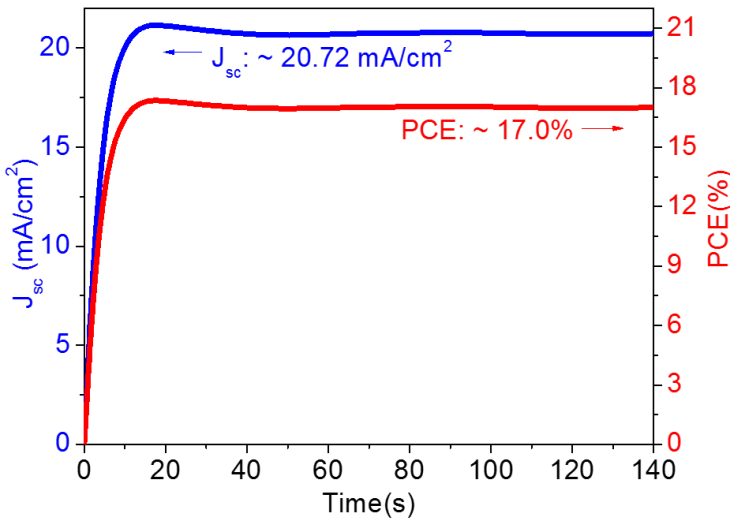

Figure S10. Stabilized photocurrent density and power output measured at the maximum power point (0.82 V) for device **D**.

S10. Photovoltaic parameters of forward and reverse scans.

Table S2. Photovoltaic parameters of forward and reverse scans with 0.1 V/s scan rate for devices **A** and **D**.

Device	Scan direction	V_{oc} (V)	J_{sc} (mA/cm^2)	FF (%)	PCE (%)	Hystersis of PCE[a]
A	Reverse	1.07	18.16	69.31	13.49	29.4%
	Forward	1.05	18.35	49.36	9.53	
D	Reverse	1.06	23.73	66.53	16.91	6.8%
	Forward	1.05	23.54	63.73	15.75	

[a] Hystersis of PCE = [PCE(reverse) - PCE(forward)]/PCE(reverse)

S11. Fitting parameters for EIS data.

Table S3. Parameters employed for the fitting of the impedance spectra of devices **A, B, C** and **D.**

Device	R_s (Ω cm^2)	R_{co} (Ω cm^2)	R_{rec} (Ω cm^2)	CPE1 (F/cm^2)	CPE2 (F/cm^2)
A	16.22	3289	9784	5.21E-8	2.95E-7
B	14.75	2343	15636	6.98E-8	9.86E-7
C	12.62	2540	17530	3.48E-7	2.51E-6
D	8.52	303	26373	2.60E-6	3.89E-6

S12. J-V curves and photovoltaic parameters of inverted perovskite solar cells based on different ETLs.

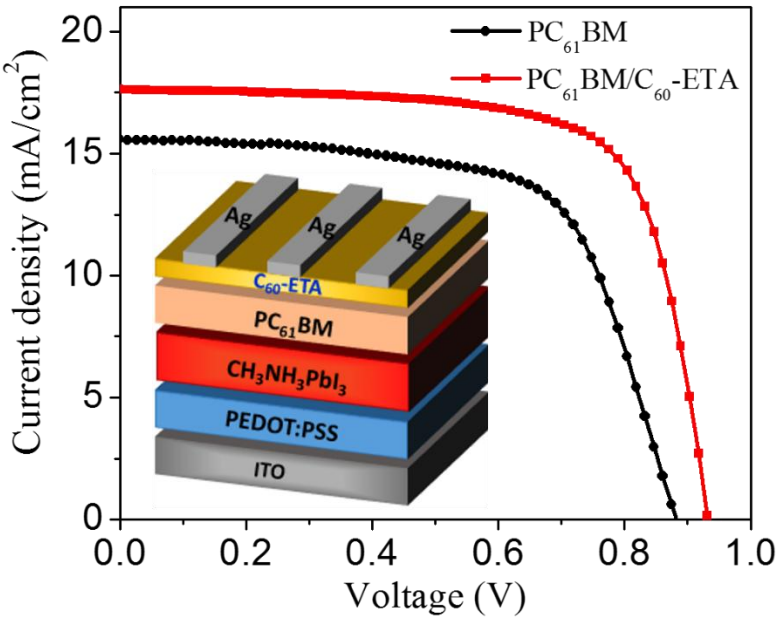

Figure S11. J−V curves of inverted perovskite solar cells containing different ETLs measured under illumination of an AM 1.5 solar simulator (100 mW•cm^{-2}) in air. The inset shows the schematic structure of the device based on $PC_{61}BM/C_{60}$-ETA ETL.

Table S4. Photovoltaic parameters of inverted perovskite solar cells containing $PC_{61}BM$ or $PC_{61}BM/C_{60}$-ETA layer as ETL.

ETL	V_{oc} (V)	J_{sc} (mA/cm^2)	*FF* (%)	PCE (%)	R_s (Ω cm^2)	R_{sh} (Ω cm^2)
$PC_{61}BM$	0.88	15.82	64.80	9.05	7.6	494.5
$PC_{61}BM/C_{60}$-ETA	0.92	17.74	72.23	11.70	3.9	1573.3

References:

S1. M. Wang, X.W. Hu, P. Liu, W. Li, X. Gong, F. Huang and Y. Cao, *J. Am. Chem. Soc.*, 2011, **133**, 9638.

S2. N. Wang, L. Sun, X.N. Zhang, X.C. Bao, W. Zheng and R.Q Yang, *RSC Adv.*, 2014, **4**, 25886.

S3. H. AitDads, S.Bouzit, L.Nkhaili , A.Elkissani and A.Outzourhit, *Solar Energy Materials & Solar Cells*, 2016, **148**, 30.